Eur. Phys. J. B **10**, 335–344 (1999)

THE EUROPEAN PHYSICAL JOURNAL B

EDP Sciences

Wetting of phospholipid membranes on hydrophilic surfaces – Concepts towards self-healing membranes

J. Nissen, S. Gritsch, G. Wiegand, and J.O. Rädler[a]

Institut für Biophysik (E22), Physik Department, Technische Universität München, James Franck Straße 1, 85747 Garching, Germany

Received 6 November 1998

Abstract. We report on the wetting behavior of phospholipid membranes on solid surfaces immersed in aqueous solution. Using fluorescence microscopy, the spreading velocity of fluid bilayers advancing from a lipid source is investigated. The kinetic spreading coefficient was measured as a function of temperature for pure DMPC membranes and as a function of charge density and cholesterol content for binary membranes. A theoretical model for the membrane flow is presented, which takes into account the liquid crystalline bilayer architecture of the lipid membrane. The spreading power results from the membrane-solid VdW interaction and is dissipated in hydrodynamic shear flow as well as by inter-monolayer friction within the bilayer. The frictional drag causes a dynamic tension gradient in the spreading membrane, which is manifested by a single exponential decay of the fluorescence intensity profile along the spreading direction. Obstacles are shown to act as pinning centers deforming the advancing line interface. However, no depinning was observed, since the centers are circumflown without abrupt relaxation.

PACS. 68.10.Gw Interface activity, spreading – 68.45.Gd Wetting – 87.16.Dg Membranes, bilayers and vesicles

1 Introduction

Substrate supported lipid membranes are a fascinating approach to biofunctionalize solid surfaces [1–4]. The phospholipid bilayer provides the natural host and binding matrix for an abundance of membrane proteins. The fixation of membrane proteins to a solid support is desired in many biotechnological as well as scientific applications for detection or imaging of the biomolecules and their ligands. Hence it is a reasonable strategy to deposit lipid membranes on solids to begin with and to incorporate functional assays therein. A variety of chemical approaches for membrane-solid coupling have been developed including silanes [3], alkylated polymer film [5] and thiolipids [6–8]. However, one physical technique, which has been successfully applied over many years is vesicle fusion [1]. The technique has the advantage of being easy to apply and to deliver membrane proteins by use of proteoliposomes [4]. On the other hand, vesicle fusion embarges the danger of producing ill-defined surfaces [9,10]. The motivation of the present paper is to investigate the forces and frictional mechanisms between lipid membranes and solids, which determine the formation of a continuous bilayer following vesicle fusion.

The construction of a continuous planar membrane *via* vesicle fusion is generally believed to follow three steps [9–11]: (i) adhesion, (ii) rupture and (iii) spreading of the vesicle membrane. The approach and adhesion of the vesicles is governed by well known colloidal interactions. For example the adhesion can be enhanced using lipids that are oppositely charged with respect to the solid surface. The rupture of vesicles depends on the lipid composition as well as the size distribution and area/volume constraints [12]. Here sonication helps to homogenize and reduce the size of the vesicles. The final step, however, the spreading, redistribution and lateral healing of ruptured membranes on the solid surface has been given little attention so far. The redistribution of lipid on a solid surface can be regarded as a "wetting" phenomenon. This fact was demonstrated by membrane spreading experiments using reflection interference microscopy [10]. The bilayer was shown to propagate in form of single bilayer sliding or in form of rolling membrane lobes, whereby only the sliding motion led to a continuous supported membrane.

In this article we describe the kinetics of lipid membrane spreading on a larger class of surfaces, including smooth hydrophilic surfaces like glass, silicon wafers or mica and rough polymer coated surfaces. The spreading coefficient was measured as a function of temperature, charge density and cholesterol content of the lipid membrane. Models for the frictional coupling to the substrate are proposed and the influence of pinning centers on lipid spreading is described. Ultimately we put forward the concept of a "self-healing membrane", which is a thermodynamic stable substrate supported membrane formed in

[a] e-mail: raedler@physik.tu-muenchen.de

the case of complete wetting on defect free surfaces. A better understanding of the wetting behavior relates to the formation and stability of supported membranes and is of importance for endeavors to design microstructured supported membranes [13,14] or electrical impedance measurements on supported membranes [15,16].

2 Theory of lipid bilayer spreading

Let us consider phospholipid that is deposited in dry, crystalline form on a hydrophilic solid surface. If the substrate is immersed in water, the phospholipid rapidly hydrates into a lamellar liquid crystalline aggregate. At the same time a single lipid bilayer spreads out to cover the bare water/solid interface. Figure 1a demonstrates the spreading of phospholipid on an oxidized silicon wafer. The membrane is doped with a small percentage of fluorescently labeled lipid in order to visualize the molecularly thin film. At the left side of the micrograph we see the overexposed lipid pool with a homogeneous spreading layer in front. The advancing membrane may be recognized as the edge of the weakly fluorescent layer reaching to the right side of the figure. Note that not the bright fingers, but the leading edge are the focus of the spreading experiment. The weakly fluorescent film corresponds to a single bilayer, which on hydrophilic surfaces slides forward on a thin lubricating hydration layer [10]. It is reasonable to assume that the leading edge of the spreading bilayer is closed by a micellar-like rim as illustrated in Figure 1b.

The lipid source can be considered a stratified droplet composed of incompressible two-dimensional fluid layers (see Fig. 1b). For the analogous case of multilayered smectic liquid crystals, it was noted by de Gennes and Cazabat that spreading occurs in a way, that only the layer adjacent to the substrate advances, while all other layers retract [17]. The classical view of a droplet with a macroscopic contact angle, however, is not applicable for membranes, since the spreading membrane exhibits an intrinsically constant thickness, d_{m}. Moreover, in contrast to a common wetting problem, where a well-defined three phase contact line exists, the membrane is fully surrounded by aqueous solvent at any instant. The advancing membrane remains separated from the solid surface by a thin water layer due to short range hydration forces. In the absence of interfacial energies the spreading power is determined by long range forces, $\Pi(z)$ from the solid (*e.g.* van der Waals). The gain in free energy per unit area is the difference in the free energy, F_{MS} between membrane and solid and the membrane-membrane energy F_{MM} within the lipid stack:

$$S = F_{\mathrm{MS}} - F_{\mathrm{MM}} \approx \int_{d_{\mathrm{h}}}^{\infty} \Pi_{\mathrm{MS}}(z)\mathrm{d}z. \qquad (1)$$

For most practical cases the spreading power of a one-component membrane can be approximated by the adhesion energy between the membrane and the substrate, which is given in equation (1) as the integral over the disjoining pressure from the equilibrium hydration layer thickness d_{h} to infinity.

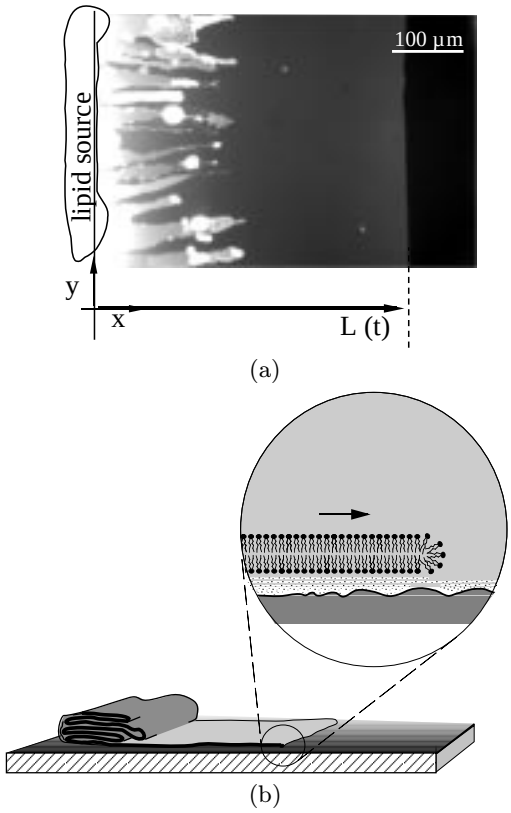

Fig. 1. (a) Fluorescence micrograph of phospholipid spreading on an oxidized silicon wafer under water. The advancing membrane is seen as a homogeneous fluorescent field with straight interface line at the right side. On the left side some additional membrane loops spill out of the source. (b) A schematic drawing of a lipid bilayer sliding on a thin water film across a hydrophilic solid surface.

The kinetics of membranes spreading from a lipid source with a straight edge can be treated as a one-dimensional problem. Let us denote the distance from the source to the leading edge of the spreading bilayer $L(t)$. It is reasonable to assume that the total spreading power S [J/m^2] will be homogeneously and isotropically dissipated over the length $L(t)$. The interfacial shear stress per unit length generated at the spreading front is balanced by a dragging force $f = \gamma_{\mathrm{s}} v(t)$ per unit area of the membrane and hence:

$$S = \gamma_{\mathrm{s}} L(t) v(t). \qquad (2)$$

Here γ_{s} [Ns/m^3] denotes the drag coefficient and $v(t) = \mathrm{d}/\mathrm{d}tL(t)$ the spreading velocity. We can integrate equation (2) and obtain the spreading velocity $v(t)$:

$$v(t) = \sqrt{\frac{S}{2\gamma_{\mathrm{s}} t}} = \sqrt{\frac{\beta}{t}} \qquad (3)$$

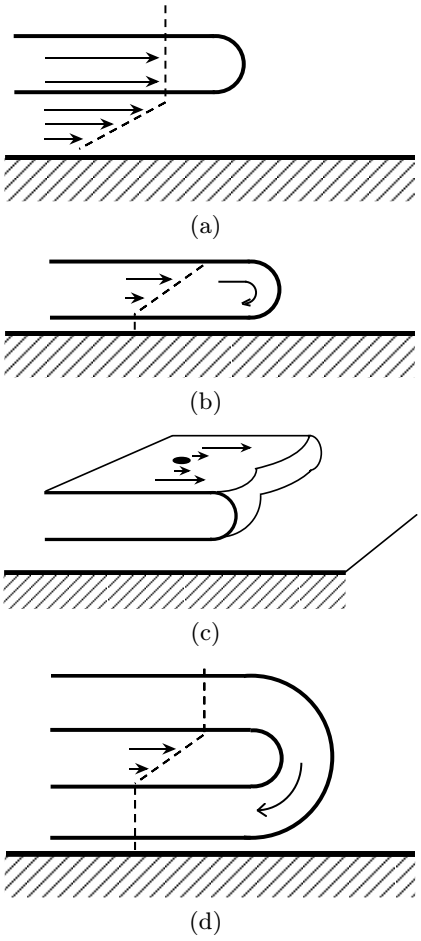

Fig. 2. Schematic sketch of the four modes of bilayer motion discussed in the text. (a) Hydrodynamic sliding of a single bilayer, (b) internal rolling with monolayer-monolayer slip (c) lateral shear flow around an embedded pinning center (d) rolling of a double bilayer lope. Note that the last type of spreading motion is topological distinct from types (a–c).

where we define $\beta = S/2\gamma_s$ as the velocity determining, *kinetic spreading coefficient* for this particular kind of spreading behavior [10].

In the following we derive the drag coefficient for three dissipative processes as schematically illustrated in Figure 2: (a) hydrodynamic slip (b) interbilayer dissipation and (c) lateral shear friction at obstacles. In the first case (a) the bilayer may be regarded as a rigid plate and the drag coefficient is simply given by the linear hydrodynamic shear flow:

$$\gamma_h = \eta/d_h. \tag{4}$$

Here d_h denotes the thickness of the lubricating hydration layer and η the viscosity of water. The second case, the interlayer dissipation (b) is properly modeled by a viscous drag coefficient $b_s = \Sigma/v^{\pm}$, with Σ [N/m^2] being an applied shear stress and $v^{\pm}$ the velocity difference of the upper and lower monolayer [18]. Since in a rolling motion the relative monolayer velocity is twice the spreading velocity $v^{\pm} = 2v_b$ the drag coefficient for inner bilayer rolling is simply:

$$\gamma_b = 2b_s. \tag{5}$$

Processes (a) and (b) may be superimposed. At constant shear stress the velocities of the inner bilayer rolling and sliding add up, $v(t) = v_a + v_b$ and the total drag coefficient γ_s is given by:

$$\gamma_s^{-1} = \gamma_h^{-1} + \gamma_b^{-1}. \tag{6}$$

So far the bilayer slipped or rolled in a constant flow field. However the membrane-substrate separation distance d_h might vary on real surfaces due to surface roughness. As a consequence of inhomogeneities shear flow will be generated in the plane of the membrane. While we leave the complete analysis of this problem to future work, we can treat the simple case of a small number of pinning centers (Fig. 2c). Let us consider a dilute concentration, c, of pinning centers per area, that pinch through or are attached to the membrane with a disk-like area of diameter a_A. The pinning centers may be regarded as cylinders which are dragged through the bilayer. The drag coefficient can be derived from the known self-diffusion constant, D_L, of the lipid molecules themselves modelled as cylinders with diameter a_L. Using the well-known Saffmann-Delbruck expression and assuming $a_A \gg a_L$ we estimate the friction γ_p due to embedded pinning centers:

$$\gamma_p \approx \frac{k_B T}{D_L} c \ln\left(\frac{a_A}{a_L}\right). \tag{7}$$

The in-plane and out-of-plane frictional coefficients can be approximately added to yield a total drag coefficient $\gamma_{total} \approx \gamma_p + \gamma_s$. Any of the three modes of motion may dominate under given circumstances. Let us compare the drag coefficients for one example of a DMPC bilayer on a flat substrate with $d_h = 10$ Å und a concentration $c = 1\ \mu\text{m}^{-2}$ of pinning centers. From micropipette and fluorescence recovery experiments on fluid DMPC bilayer it is known that $b_s = 3\times10^7$ N s/m^3 and $D_L = 10\ \mu\text{m}^2/\text{s}$ [18, 19]. Hence with $\eta(\text{water}) = 10^{-3}$ kg/sm we finally have $\gamma_h = 10^6$ N s/m^3, $\gamma_b = 6\times10^7$ N s/m^3 and $\gamma_{pinning} \approx 10^3$ N s/m^3 using equations (4, 5, 7), respectively. We may conclude that in this case the drag of pinning centers can be neglected. According to equation (6) the hydrodynamic drag dominates for any realistic thickness of the hydration layer $d_h > d^* = \eta/2b_s \approx 0.3$ Å as long as hydrodynamic slippage occurs. Note that this estimate for d^* is purely theoretical and that the real cross-over from hydrodynamic slip to bilayer rolling will be determined by the critical spacing down to which the hydrodynamic flow is appropriately described by equation (4). The limits of the hydrodynamic model is best explored experimentally. Hence for bilayer spreading experiments a useful distinction can be drawn between the sliding (slip) and inner bilayer rolling (non-slip) condition with the measurable spreading coefficient given by:

$$\beta = Sd_h/2\eta \quad \text{sliding,} \tag{8a}$$

$$\beta = S/b_s \quad \text{rolling.} \tag{8b}$$

Finally a topologically distinct form of membrane motion exists that is shown in Figure 2d. A double bilayer lope can roll forward in a tank thread-like motion. The observation and analysis of this motion has been made previously [20]. It was found that the velocity for the straight interface geometry is constant $v = 2S/\pi b_s d_m$ with the frictional force most likely being determined by interbilayer slip at the bent leading edge. The sliding of a single bilayer and rolling of double-bilayer fingers compete in every spreading experiment and may be found to coexist, if the resulting spreading velocities are comparable.

3 Experimental section

3.1 Substrate cleaning

Glass cover slides were purchased from Zefa (Munich, Germany). Silicon wafers with 150 nm oxide layer were kindly provided by Wacker (Burghausen, Germany). All substrates were carefully cleaned twice by ultrasonication for half an hour in a detergent solution (2 % Hellmanex, Hellma, Germany), subsequently thoroughly rinsed and ultrasonicated in pure millipore water at 40 °C. Finally the substrates were dried in an oven at 90 °C.

3.2 Membrane preparation

All lipids were obtained from Avanti Polar Lipids (Birmingham, Al). Texas Red DHPE (582/601), BODIPY phospholipid (581/591) and BODIPY fatty acid (542/563) was delivered from Molecular Probes (Eugene, OR). If not mentioned otherwise the lipids were dissolved in chloroform at a concentration of 1 mg/ml and mixed with 0.02 mol % Texas Red DHPE. The lipid/chloroform solution was deposited on the edge of a Teflon block and dried over night in vacuum. Before the experiment, lipid was transferred by imprinting (smearing) lipid from the Teflon block on to the substrate. Care was taken to obtain lipid deposits with straight edges. The sample was then mounted in a temperature controlled chamber. After half an hour for equilibrating the temperature in the dry chamber the spreading process was started by adding water of equal temperature.

3.3 Polymer films

Ultrathin dextrane films were chemically grafted to the glass surface coated with epoxylated silanes as previously described [21]. The dextrane films have thicknesses between 2 Å and 30 Å in the dry state and between 600 Å and 800 Å in the fully hydrated state as measured by ellipsometry. Regenerated cellulose layers were prepared from monolayers of hairy rods by Langmuir Blodgett technique [5]. In the experiments on dextran and cellulose films lipid was not deposited from a chloroform solution, but rather put in dry, crystalline form onto the substrate.

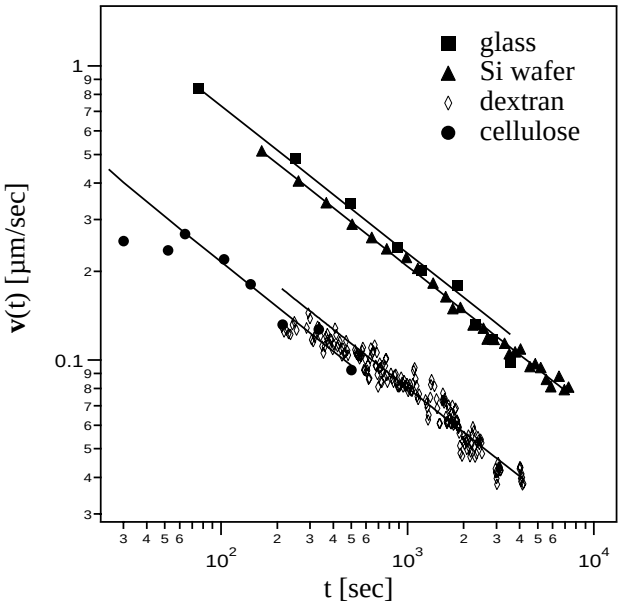

Fig. 3. A log-log plot of the spreading velocity as a function of time for different surfaces: silicon wafer (▲), glass (■), dextran coated glass (◊) and cellulose coated glass (●). The velocities follow a power law $v = (\beta/t)^{1/2}$. The straight lines are best fits with slope $-1/2$.

3.4 Image acquisition and processing

In the case of fluorescence microscopy the spreading front was observed with a Zeiss Axiovert 135-TV (Zeiss, Jena, Germany) using a Plan Neofluar 10× (NA 0.3) and a 40× (NA 0.75) objective, high pressure mercury lamp HBO 100 (Osram) and a Zeiss dicroic filter set (FT00). Fluorescence images were taken with a 12 bit digital CCD-Camera (MicroMax, Princeton Instruments, Trenton, USA). The velocity of the spreading front was determined using IPLab software (Signal Analytics Corporation, Vienna, Austria).

The spreading experiments on polymer films were carried out on glass with an optical interference coating, MgF_2/SiO_2 (63 nm/25 nm). In this case the spreading front was imaged using reflection interference microscopy as described previously [10,22].

4 Results and discussion

4.1 Spreading kinetics

The spreading kinetics of fluid membranes were measured for various hydrophilic surfaces. Figure 3 shows the flow velocities of DMPC on glass, silicon wafer, regenerated cellulose and dextran layers respectively. The velocities are plotted in a log-log presentation as a function of time. Independent of the nature of the surfaces the velocities decreases with the power law dependence predicted by equation (2). The straight lines in the log-log representation are best fits with slope $-1/2$. The resulting prefactors, the kinetic spreading coefficients, β are listed in Table 1.

Table 1. The kinetic spreading coefficient of DMPC at $T = 30\,^{\circ}\mathrm{C}$.

	spreading coefficient [$\mu\mathrm{m}^2/\mathrm{s}$]
cover glass	26 ± 3
silicon waver	37 ± 5
mica	43 ± 5
cellulose	5.2 ± 0.5
dextran	6.5 ± 0.5

Let us assume that the spreading coefficients are described by the bilayer sliding model. In the case of glass surfaces we know from neutron reflectivity measurements that the thickness of the water film between supported DMPC membranes and glass is $d_\mathrm{h} \approx 20$ Å [23]. It is instructive to estimate the spreading power $S = d_\mathrm{h}/2\beta\eta_\mathrm{h} \approx 10^{-4}$ J/m^2 in this case with the measured spreading coefficient $\beta \approx 30\ \mu\mathrm{m}^2/\mathrm{s}$. The order of magnitude of S is in good agreement with the expected adhesion energy due to van der Waals interaction:

$$W_\mathrm{VdW} = -\frac{A_\mathrm{H}}{12\pi}\,\frac{1}{d^2} \tag{9}$$

which for $d_\mathrm{h} = 20$ Å is $W_\mathrm{VdW} = 0.7 \times 10^{-4}$ J/m^2 given a Hamaker constant $A_\mathrm{H} = 10^{-20}$ J/m^2 [24]. Hence the spreading rates are well described by the spreading law equations (8a, 1). In agreement with this model similar spreading coefficients are observed for DMPC on the chemically related glass, silicon wafer and mica surfaces (see Tab. 1).

The sliding model may furthermore be applied to lipid membrane spreading on tethered polymers. We have chosen hydrophilic polymers which do not interact with the lipid membrane specifically but keep the membrane further away from the solid due to the repulsive steric force of the random polymer coils. To first approximation in a dilute polymer mesh the VdW and hydrodynamic interaction is little affected. Hence the spreading coefficient $\beta \sim W_\mathrm{VdW}\, d_\mathrm{h}/\eta_\mathrm{eff} \sim A_\mathrm{H}/\eta_\mathrm{eff}\, d_\mathrm{h}$ depends inversely proportional on the membrane substrate separation distance. The observed spreading rates would then be in agreement with an estimated 100 Å membrane-solid separation.

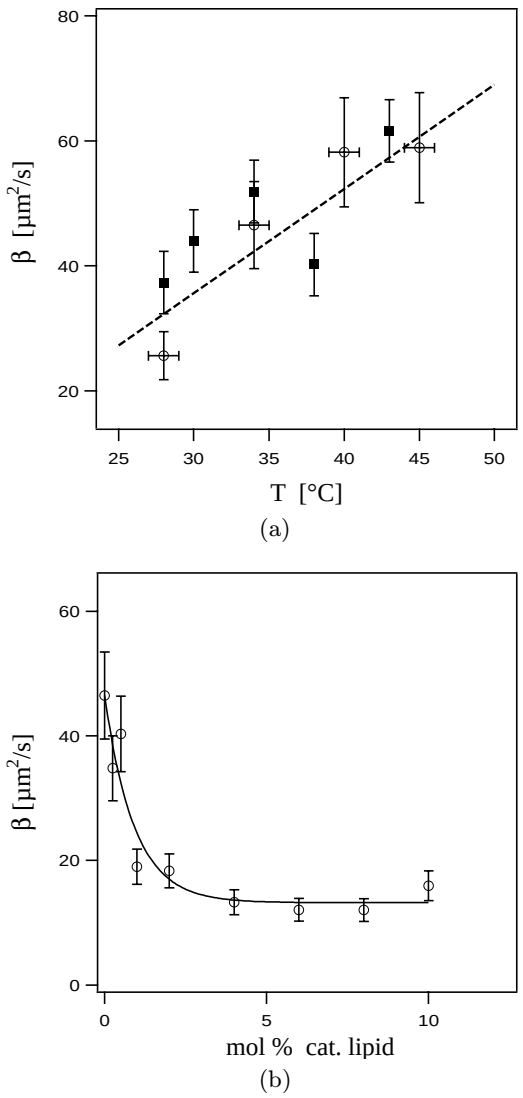

Fig. 4. (a) Dependence of the kinetic spreading coefficient β of a DMPC membrane on the temperature. The straight line indicates a linear fit. (b) The kinetic spreading coefficient as a function of the molar fraction of a cationic lipid additive at $T = 35\,^{\circ}\mathrm{C}$. The full line is added to guide the eye.

4.2 Temperature dependence of spreading

In order to find further quantitative proof for equation (8a) we performed experiments as a function of temperature and as a function of charge density. A substantial increase in the spreading coefficient with temperature is found even in the small temperature range accessible for spreading experiments. Figure 4a depicts the values for DMPC on glass (white dots) and silicon wafers (black dots). The increase in the spreading coefficient is linear within the accuracy of the experiment. The dashed line represents a linear fit with thermal coefficient

$$\alpha = \frac{1}{\beta_0}\,\frac{\partial\beta(T)}{\partial T} = 0.06\ K^{-1} \tag{10}$$

where we set $\beta_0 = \beta\ (28\,^{\circ}\mathrm{C})$. Within the sliding model the temperature dependence must be due to a change in the water viscosity, the membrane substrate separation distance or the spreading power. The strongest temperature dependence is expected to stem from the water viscosity $\eta(T)$. The predicted linearized thermal coefficient corresponding to the bulk viscosity of water is $\alpha_\eta = 0.03\ K^{-1}$ and accounts only for half the observed effect. We speculate that the stronger temperature dependence is due to partial structuring of water in the hydration layer leading to a higher temperature dependence than reported for bulk water.

4.3 Spreading of charged membranes

We performed experiments on binary membranes composed of neutral phospholipids (DMPC) and cationic lipids (DMTAP), which are electrostatically attracted to the negatively charged glass surface. The simple spreading law, equation (8a), predicts that the spreading coefficient might rise with increasing adhesion energy. Figure 4 shows the measured spreading coefficients as a function of mol percentage charged lipid. To our surprise the spreading velocity drops by a factor of 2 and remains almost constant for charge fractions larger than 3 %.

It is idle to discuss the sliding model in great detail without knowing the change in the water layer spacing. However we like to point out that a binary membrane is free to redistribute its components. The spreading power can no longer be approximated by an adhesion energy alone, but contains entropic terms of demixing. As described recently in a seminal paper on the adhesion of cationic vesicles to anionic substrates, the regulated charge redistribution of the mobile cationic lipids has dramatic consequences and leads in particular to the failure of the classical Young-Dupré law [25].

Interestingly we observe a transition from a linear to a constant spreading regime at a lipid charge density, which exactly corresponds to the surface charge of glass. For equal but opposite charge densities the classical Poisson Boltzmann theory predicts the maximum adhesion [26]. For charge densities of the membrane exceeding the substrate charge density a constant spreading power independent of the mol fraction cationic lipid in the membrane is predicted due to charge regulation at the leading edge [25]. The fact that the spreading coefficient decreases rather than increases with higher mol fraction cationic lipid might be explained by the fact that the membrane substrate spacing decreases beyond the limit of the simple hydrodynamic model.

4.4 Imaging the tension gradient

We observed that the fluorescence intensity profile along the spreading direction showed enhanced fluorescence at the leading edge of the membrane in all experiments, where a Texas Red DHPE lipid label was used. As shown in Figure 5a the intensity is well fitted by a single exponential decay at all times:

$$I(x,t) \cong I_0 \exp(-x/\lambda) + \text{const.} \tag{11}$$

The exponential intensity profile was found to be independent of the substrate and the lipid composition.

The enhanced fluorescence at the leading edge of the membrane is rather surprising. One might expect on the contrary that the bulky fluorophore is retarded by hydrodynamic forces. In the following we propose a steady state model, that assumes that the fluorescence label experiences elastic forces due to a small density gradient in the sliding membrane. The hydrodynamic shear flow between the lipid membrane and the solid causes shear stress which acts on the lower side of the membrane. This shear stress is balanced by an elastic tension, σ [N/m], at each point. At the leading edge this elastic tension must equal the spreading power. Hence in a dynamic spreading experiment the internal membrane tension is not constant but rather decreases linearly from the leading edge to the lipid pool:

$$\sigma(x,t) = S\frac{x}{L(t)} \quad \text{for} \quad 0 < x < L. \tag{12}$$

The membrane tension causes an area dilation $\mathrm{d}A/A = \sigma/K$ with K being the lateral area compressibility of the fluid lipid membrane. We assume that the fluorescently labeled tracer molecules prefer a lower lipid density with energetic advantage $\Phi = \varepsilon\,\mathrm{d}A/A$. Hence an elastic potential is given by:

$$\Phi(x,t) = \varepsilon\frac{\sigma}{K} = \frac{\varepsilon S}{KL(t)}x \tag{13}$$

where ε denotes the coupling constant. In a steady state the lipid will redistribute in a stable profile and the fluorescence intensity is accordingly proportional to the Boltzmann distribution:

$$I(x,t) = I_0 \exp\left(\frac{-\Phi(x,t)}{kT}\right) = I_0 \exp\left(\frac{-x}{\lambda}\right) \tag{14}$$

with:

$$\lambda = \frac{KkT\,(\beta t)^{1/2}}{\varepsilon S}. \tag{15}$$

This model is supported by two experimental observations. First of all the predicted time dependence of the fluorescence decay length was verified as shown in Figure 5b. Secondly, we tested different fluorescence labels and found that each fluorescence label follows equation (14) but with different coupling constants ε. As shown in Figure 5c Texas Red labeled DHPE showed the strongest segregation, while BODIPY chain labeled PC exhibited a reduced tendency to redistribute. Most interestingly BODIPY labeled fatty acid revealed a reversed fluorescence distribution indicating that the relatively small amphiphile prefers areas of high lipid density.

It is worthwhile to calculate the typical area dilation. Using $K = 0.14$ N/m [27] and $S = 10^{-4}$ J/m^2 we obtain $\alpha = 10^{-3}$ Hence from the measured decay length $\lambda(t)$ we conclude $\varepsilon \approx 10^4\ kT$ for Texas Red DHPE. This value might appear extremely large. However it has to be looked at with respect to the chemical potential difference of lipid monomers in the bilayer and in bulk water. The hydrophobic effect is larger by more than a factor 4. We conclude that Texas Red DHPE might indeed be a very sensitive sensor for density variations within the lipid membrane.

4.5 Effect of cholesterol

Besides phospholipids cholesterol is the most abundant component in natural membranes. In the following we describe the wetting behavior of DMPC-cholesterol mixtures

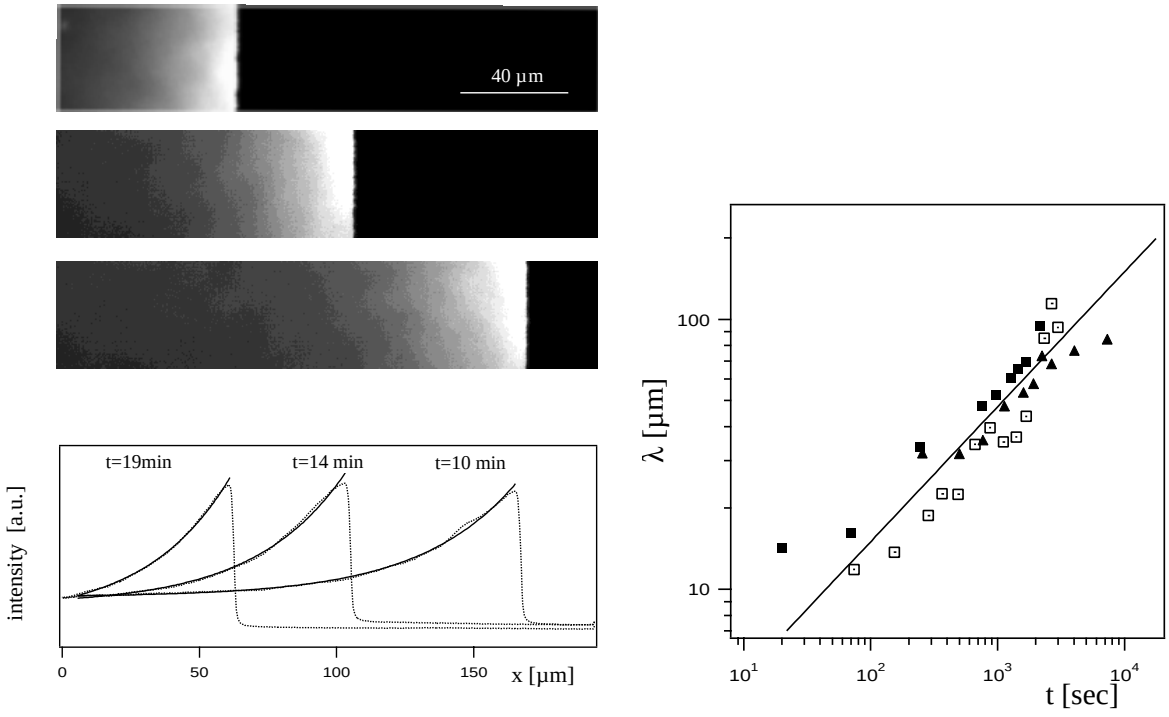

(a) (b)

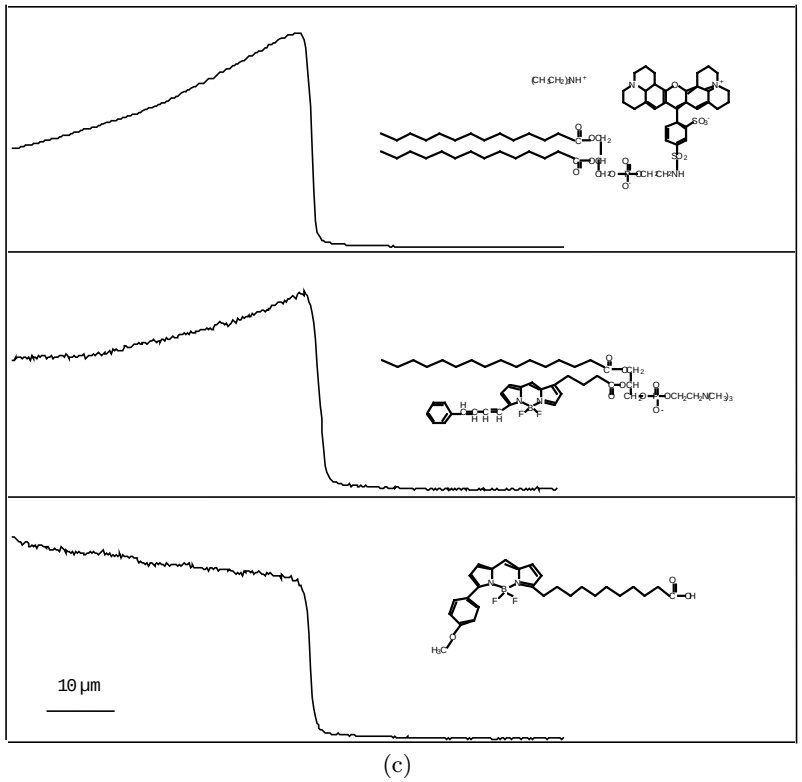

(c)

Fig. 5. (a) Time sequence of the advancing lipid bilayer and the corresponding intensity contour plots. The fluorescence intensity is enhanced at the leading edge of the membrane and decays exponentially towards the lipid source. (b) Scaling of the decay length, λ, with time. The straight line indicates slope 1/2. Three spreading experiments of DMPC on glass (■, □) and on silicon wafer (▲) at $T = 30\,^{\circ}\mathrm{C}$ are shown. (c) Intensity profile for three different fluorescence labeles (A) Texas Red DHPE (B) chain labeled BODIPY phospholipid and (C) BODIPY fatty acid. The dyes are distinct in their headgroup to chain volume ratio.

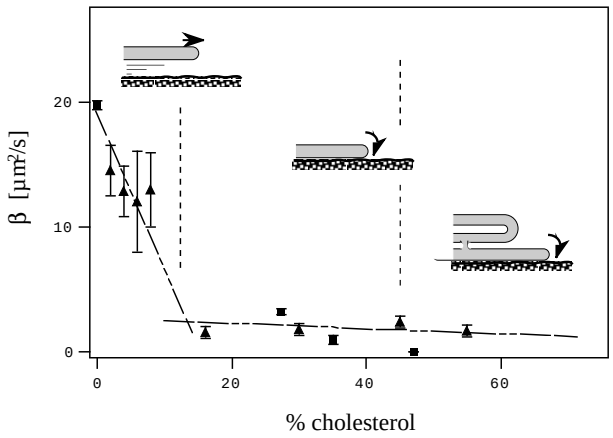

(a)

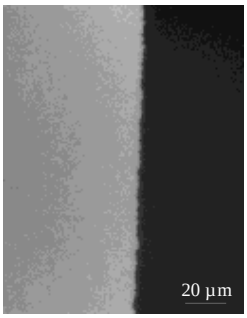

(b)

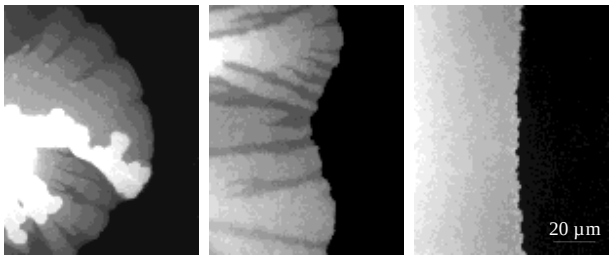

(c)

Fig. 6. (a) The kinetic spreading coefficient β of DMPC on glass decreases with increasing cholesterol content and exhibits a transition from sliding to rolling. (b) Fluorescence image of the spreading front for 4 mol % cholesterol (sliding regime). (c) Three micrographs as a function of time 7 min, 36 min, 62 min for a DMPC-cholesterol (1:1) membrane on glass. The lipid bilayer fingers on top of the advancing single bilayer slowly fuse into the underlying membrane.

on glass. As shown in Figure 6a the measured spreading behavior can be distinguished in three regimes as a function of increasing cholesterol content. At low cholesterol content bilayer sliding is observed with the spreading coefficient decreasing monotonously by more than a factor 10 (see also Fig. 6b). The minimum spreading coefficient is reached at about 10 mol %, where a second regime of constant spreading coefficient follows. Finally at cholesterol contents of about 40 % rolling of double bilayer lobes on top of the spreading single bilayer sets in. However the bilayer fingers fuse into the underlying lipid bilayer over some time and finally exhibit a single bilayer front as seen in the previous regimes (see time sequence in Fig. 6c).

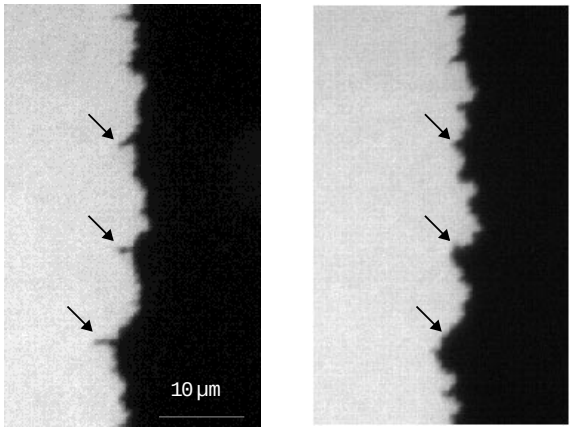

Fig. 7. Demonstration of line pinning for DMPC spreading on a glass surface. The arrows in the left micrograph indicate the location of defects compared to the same spot 30 seconds later (right micrograph). No abrupt depinning is observed. The obstacles are rather circumflowed.

We interpret the decrease of the spreading coefficient by a continuous dehydration of the membrane substrate water gap. Eventually the frictional coupling to the substrate becomes so strong that the inner bilayer rolling (Fig. 2b) dominates. In fact the latter is in quantitative agreement with the spreading coefficient as described by equation (8b) using $b_s = 3 \times 10^7$ Ns/m^3 and $S = 1 \times 10^{-4}$ J/m^2 [18,19].

It is noteworthy that both transition points coincide with phase boundaries in the DMPC/cholesterol phase diagram. At 10 mol % the coexistence region of the liquid disordered and the liquid ordered phase begins, while at 30 mol % the phase boundary to the pure liquid ordered phase is reached [28]. Obviously the spreading behavior of the liquid ordered phase is qualitatively different from the single bilayer spreading, since two adjacent bilayers seem to communicate and exchange lipid. The bilayer fingers seem to slowly fuse into lowest bilayer, suggesting the formation of stalk-like pores.

4.6 Spreading with obstacles

So far we have assumed that the advancing line interface is straight. However real surfaces expose obstacles, which act as pinning centers for the advancing membrane rim. Surface heterogeneities are well known in wetting experiments and manifest themselves in contact angle hysteresis and contact line distortions [29]. Figure 7 demonstrates the existence of pinning centers for membranes on cover slides. The membrane contact line is retarded by defects as indicated by arrows in Figure 7a and subsequently circumflowed by closure of the membrane behind the obstacle (Fig. 7b). No depinning or rapid relaxation of the line contour is observed.

The existence of pinning centers can be rationalized as submicron dust particles. However, there exists a

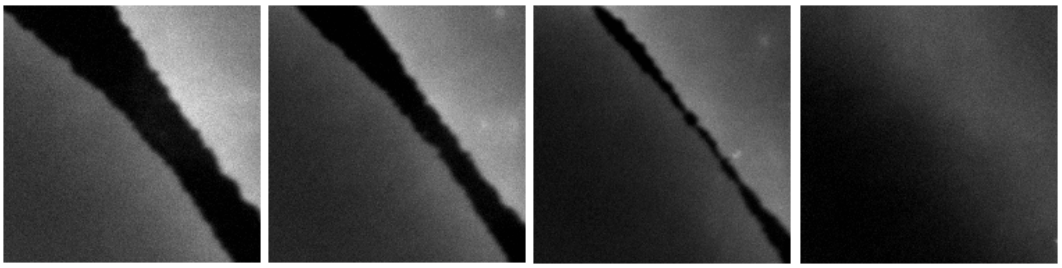

Fig. 9. Two interfaces of single bilayer meet and fuse into a continuous planar membrane. In this sense a supported membrane wetting a solid surface is self-healing.

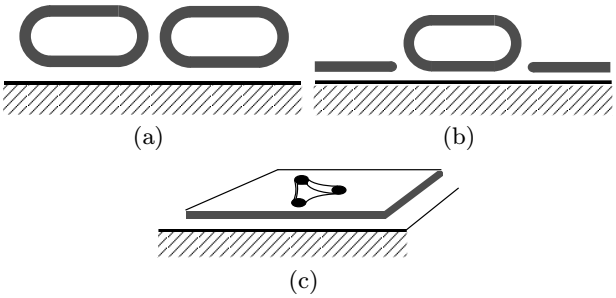

Fig. 8. Schematic illustration of possible imperfections after vesicle fusion. (a) Two unruptured vesicles, (b) unruptured vesicle blocking a continuous single bilayer (c) pinning centers preventing the closing of a single bilayer.

fundamental difference in the way obstacles are overcome by a membrane in contrast to classical pinning and depinning of a three dimensional droplet on solids. In three dimensions a pinned liquid interface increases the interface area with the square of the length of the distortion. An effective elastic force acts on the pinning center that linearly increases with the length of the distortion [30]. At a certain threshold force the interface depins and the contact line moves rapidly forward. The lipid membrane, in contrast, forms a two-dimensional liquid with a one-dimensional interface. The interface exhibits a line tension, that arises from the free energy cost of the micellar shaped edge growing with the contour distortion. Hence a pinning center experiences a constant force. This explains the observation that no depinning exist for bilayer spreading and that the obstacles are rather circumflowed.

However a large number of pinning centers should hinder and eventually stop membrane spreading. Simple two-dimensional models of fluid invasion into porous media predicting critical percolation thresholds are applicable to the case of membrane spreading [31,32]. These models are in particular useful, since the line interface was found to be self-affine [10]. For a given spreading parameter stable arcs of radius Θ/S must form between two pinning centers, whereby Θ denotes the one-dimensional line tension. The percolation threshold of the invasion process will critically depend on the contact angle that is formed in the plane of the solid surface between the membrane rim and the defect. However the line deformations are most likely not resolvable by optical microscopy, since the line tension is estimated to be smaller than $\Theta = 10^{-10}$ J/m [33]. Experiments to test spreading at defined pinning center are in progress.

4.7 Self-healing and vesicle coating

A positive spreading power drives the membrane to cover the solid until the lipid source is exhausted or the solid is completely coated. Why then is it so difficult for most practical purposes to obtain membrane coated surfaces? In previous studies the failure of vesicle fusion was shown to be due to adsorbed but not ruptured vesicles [11,34]. In Figure 8a this situation is sketched schematically. Adsorbed vesicles might also coexist with single bilayer patches as a result of incomplete vesicle fusion (Fig. 8b). Likewise the existence of a large density of pinning centers can result in uncoated areas as shown in Figure 8c. Spreading experiments help to estimate the likelihood of these kind of defects. A large spreading coefficient will generally also favor vesicle fusion. The experience that freshly cleaned and hydrophilized surfaces yield better coatings by vesicle fusion is manifested in large spreading coefficients. Cholesterol-rich membranes on the other hand are an example, where the spreading coefficient is small but yet very good coatings can be achieved by vesicle fusion. In this case the property of cholesterol-rich membranes to easily fuse with each other, as seen in spreading experiments (Fig. 6c), is the dominating effect.

Sequences of fusing membrane fronts, like the one shown in Figure 9, have lead us think of supported membranes as "self-healing" membranes. In principle this means that a membrane, which is accidentally scratched will re-seal by spreading, if some lipid reservoir exists. Yet, in practice it can be observed, that mechanical scratches may act as effective diffusion barriers, which prevent the healing of the supported membrane [13,14]. This observation, however, does not conflict with the idea of a self-healing membrane, since mechanical scratches are often accompanied by the creation of topological faults in the solid surface around the scratch, which prevent the membrane to heal [35,36]. On smooth surfaces the "self-healing" property is rather desirable for example in case of biomembranes used as coatings in electrical impedance measurements on solid electrodes. Patch clamp experiments for example often suffer from mechanical instability of freely suspended model membranes [16]. A supported

membrane on the other hand, which is composed to optimally wet a solid electrode should exhibit good mechanical stability. We found that large spreading coefficients are not necessarily related to higher electrical resistance, *e.g.* DMPC shows a larger spreading coefficient on ITO electrodes but lower resistance than a 1:1 DMPC-cholesterol mixture. But the addition of a small percentage cationic lipid (DHDAB) increases the spreading coefficient of the 1:1 DMPC-cholesterol mixture and results in an even higher impedance of the supported membrane [15]. Currently lipid membrane seals with specific resistance as high as 500 k Ohm/cm^2 can be achieved on solid electrodes.

5 Conclusions

We showed that the kinetics of bilayer spreading follows a universal spreading law, which allows to compare the kinetic spreading coefficients for various surfaces and to study the dependence on membrane composition. The proposed spreading model describes three contributions to the frictional drag on a single homogeneous bilayer and is consistent within the set of data presented here. In particular the transition from a bilayer sliding motion to an inner bilayer rolling distinguishes strongly hydrated surfaces from hydrophilic but less hydrated surfaces. Further experiments will have to proof the soundness of the model. More importantly the behavior of binary membranes strongly indicates a possible demixing of the spreading bilayer and the bilayer in the feeding lipid source. The observed exponential distribution of the fluorescence tracer is an example for a steady state redistribution, which was shown to be due to a dynamic tension gradient in the membrane. Such effects might be observable in many other dynamic membrane experiments and should increase the caution necessary for quantitative interpretation of fluorescence.

Two aspects of this work are of practical importance. Firstly, the kinetic spreading coefficient might proof useful as an indicator for the ability of supported membranes to heal by complete wetting. And secondly the study of surface defects on the wetting behavior of membranes is shown to be crucial in the understanding of the self- organisation of lipid membranes on solids in general and the electrical resistance of membranes on solid electrodes in particular.

We thank E. Sackmann, J. Nardi and R. Merkl for helpful discussions. This work was funded by DFG grants Ra655/2-1 and Ra655/3-1.

References

1. E. Sackmann, Science **271**, 43 (1996).
2. H.M. McConnell, T.H. Watts, R.M. Weis, A.A. Brian, Biochim. Biophys. Acta **864**, 95 (1986).
3. D. Beyer, G. Elender, W. Knoll, M. Kühner, S. Maus, H. Ringsdorf, E. Sackmann, Angew. Chem. Int. Ed. Engl. **35**, 1682 (1996).
4. J. Salafsky, J.T. Groves, S.G. Boxer, Biochemistry **35**, 14773 (1996).
5. G. Wiegand, T. Jaworek, G. Wegner, E. Sackmann, Langmuir **13**, 3563 (1997).
6. H. Lang, C. Duschl, H. Vogel, Langmuir **10**, 197 (1994).
7. S. Lingler, I. Rubinstein, W. Knoll, A. Offenhäuser, Langmuir **3**, 7085 (1997).
8. B. Raguse, V. Braach-Maksvytis, B.A. Cornell, L.G. King, P.D.J. Osman, R.J. Pace, L. Wieczorek, Langmuir **14**, 648 (1998).
9. P. Nollert, H. Kiefer, F. Jähnig, Biophys. J. **69**, 1447 (1995).
10. J.O. Rädler, H. Strey, E. Sackmann, Langmuir **11**, 4539 (1995).
11. E. Kalb, S. Frey, L.K. Tamm, Biochim. Biophys. Acta **1103**, 307 (1992).
12. R. Lipowsky, U. Seifert, Mol. Cryst. Liq. Cryst. **202**, 17 (1991).
13. J.T. Groves, N. Ulman, S.G. Boxer, Science **275**, 651 (1997).
14. A.T.A. Jenkins, R.J. Bushby, N. Boden, S.D. Evans, P.F. Knowles, Q. Liu, R.E. Miles, S.D. Ogier, Langmuir **14**, 4675 (1998).
15. S. Gritsch, P. Nollert, F. Jähnig, E. Sackmann, Langmuir **14**, 3118 (1998).
16. C.A. Steinem, A. Janshof, W.-P. Ulrich, M. Sieber, H.-J. Galla, Biochim. Biophys. Acta. **1279**, 169 (1998).
17. P.-G. de Gennes, A.-M. Cazabat, C.R. Acad. Sci. Paris II **310**, 1601 (1990).
18. E. Evans, A. Yeung, Chem. Phys. Lipids **73**, 39 (1994).
19. R. Merkel, E. Sackmann, E. Evans, J. Phys. France **50**, 1535 (1989).
20. T.J. Feder, G. Weissmüller, B. Zeks, E. Sackmann, Phys. Rev. E **51**, 3427 (1995).
21. G. Elender, M. Kühner, E. Sackmann, Biosens. Bioelectron. **11**, 565 (1996).
22. J. Rädler, E. Sackmann, J. Phys. II France **3**, 727 (1993).
23. S.J. Johnson, T.M. Bayerl, D.C. McDermott, G.W. Adam, A.R. Rennie, R.K. Thomas, E. Sackmann, Biophys. J. **59**, 289 (1991).
24. J.N. Israelachvilli, *Intermolecular and Surface Forces* (Academic Press, London, 1991).
25. J. Nardi, R. Bruinsma, E. Sackmann, Phys. Rev. E **58**, 6340 (1998).
26. V.A. Parsegian, D. Gingell, Biophys. J. **12**, 1192 (1972).
27. E. Evans, D. Needham, J. Phys. Chem. **91**, 4219 (1987).
28. P.F.F. Almeida, W.L.C. Vaz, T.E. Thompson, Biochemistry **31**, 6739 (1992).
29. L. Leger, J.F. Joanny, Rep. Prog. Phys. **431** (1992).
30. P.-G. de Gennes, Rev. Mod. Phys. **57**, 827 (1985).
31. M.A. Rubio, C.A. Edwards, A. Daugherty, J.P. Gollub, Phys. Rev. Lett. **63**, 1685 (1989).
32. N. Martys, M. Cieplak, M.O. Robbins, Phys. Rev. Lett. **66**, 1058 (1991).
33. E. Sackmann, FEBS Lett. **346**, 3 (1994).
34. C.A. Keller, B. Kasemo, Biophys. J. **75**, 1397 (1998).
35. P.S. Cremer, S. Boxer, J. Phys. Chem. B **103**, 2554 (1999).
36. P.S. Cremer, J.T. Groves, L.A. Kung, S. Boxer, Langmuir **15**, 3893 (1999).